Design of Drives for Inverter-Assisted Induction Generators

Max Myers, Marc Bodson, and Faisal Khan

***Abstract*—This paper investigates the control of power generation using two-phase squirrel-cage induction machines, where the load is connected to one stator winding and the load voltage is controlled through the other winding. The concept can be applied to three-phase machines as well. A state-space model of the machine is used to identify suitable operating regions. Then, two types of control algorithms are proposed: The first type regulates the frequency and the magnitude of the generated voltage and is suitable for stand-alone operation. The second type also regulates the phase of the voltages, enabling grid synchronization. Experimental results are presented for each of the control algorithms. The closed-loop systems are found able to track the desired reference and to reject disturbances caused by significant changes in load and speed.**

***Index Terms*—Adaptive control, induction machines, motor drives, power generation, renewable energy.**

NOMENCLATURE

$v_{SA}, v_{SB}, v_{RX}, v_{RY}$	Stator and rotor voltages.
$i_{SA}, i_{SB}, i_{RX}, i_{RY}$	Stator and rotor currents.
R_A, R_B, R_R	Stator and rotor resistances.
L_A, L_B, L_R	Stator and rotor inductances.
M_A, M_B	Mutual inductances.
n_p	Number of pole pairs.
θ	Rotor position.
ω	Rotor velocity.
ω_e	Electrical frequency.
R	Load resistance.
C	Load capacitance.
Subscript A	Auxiliary winding.
Subscript B	Main winding.
Subscript R	Rotor.

I. INTRODUCTION

SQUIRREL-CAGE induction machines are inexpensive, low maintenance, and lightweight, which makes them attractive for power generation from renewable sources such as wind and hydro. Recent concerns over the availability of rare-earth materials add to the benefits of induction machines, compared to permanent-magnet generators. In this paper, we consider the use of off-the-shelf squirrel-cage induction motors for power generation. At the low power level considered here, split-phase induction motors are typical. At higher power levels, three-phase machines dominate.

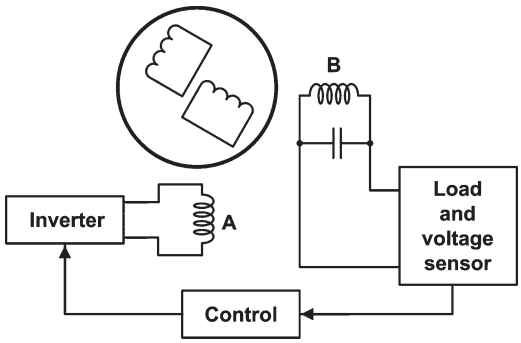

Fig. 1. Inverter-assisted induction generator.

Induction machines can be used for power generation in multiple ways. Wound-rotor induction machines are the most flexible, and their ability to operate over a wide range of speeds makes them attractive for wind power. However, their cost is prohibitive at lower power levels. The generation of power using squirrel-cage induction generators operating on a dc bus with a voltage source inverter was proposed in [1]. Power generation is also possible in the self-excited mode [2], [3], i.e., without any external power source. However, it is difficult to exploit due to the inherent instability and nonlinearity of the self-excitation phenomenon [4].

An interesting alternative to generating power with squirrel-cage induction machines was proposed in [6]. The principle is shown in Fig. 1, and the scheme is usually referred to as an *inverter-assisted induction generator*. Fig. 1 shows the example of a split-phase induction machine, where an inverter controls the auxiliary winding (labeled A) and power is generated on the main winding (labeled B). A capacitor is placed in parallel with the main winding to provide the reactive power needed (thereby reducing the current in the auxiliary winding). A control law regulates the voltage and frequency on the load through proper adjustment of the inverter signals.

The approach presents several interesting features.

1) With sinusoidal excitation, the frequency of the voltage on the load is the same as the frequency of the voltage applied by the inverter.
2) A constant frequency can be applied to the load for some range of speeds (asynchronous operation).
3) The amplitude of the voltage on the load is approximately proportional to the voltage applied to the inverter so that regulation of the load voltage is possible.

Manuscript received December 1, 2011; revised April 25, 2012; accepted May 26, 2012. Date of publication October 26, 2012; date of current version December 31, 2012. Paper 2011-661.R1, approved for publication in the IEEE TRANSACTIONS ON INDUSTRY APPLICATIONS by the Industrial Drives Committee of the IEEE Industry Applications Society.

M. Myers is with Boulder Wind Power, Boulder, CO 80301 USA (e-mail: maxrmyers@gmail.com).

M. Bodson and F Kahn are with the Power Electronics and Automation Research Laboratory (PEARL), Department of Electrical and Computer Engineering, University of Utah, Salt Lake City, UT 84112 USA (e-mail: bodson@eng.utah.edu; faisal.khan@utah.edu).

Digital Object Identifier 10.1109/TIA.2012.2226693

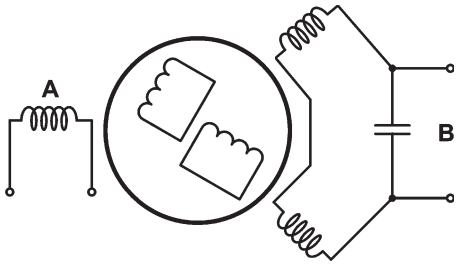

Fig. 2. Inverter-assisted three-phase induction generator.

4) The harmonic content of the voltage applied to the load is smaller than the harmonic content applied to the auxiliary winding, due to the filtering provided by the machine.
5) Only one inverter is needed to generate power from two windings.

The effect of different loadings on the generator's performance was explored in [7], and the effect of more advanced modulation schemes was studied in [8]–[10]. The inverter–generator topology was used to identify the parameters of an induction machine in [11].

The problem of designing a closed-loop system to regulate the generated voltage was not addressed until very recently [12]. An interesting contribution of this paper is to show that the inverter-assisted scheme can be used to generate single-phase power using a three-phase machine, using the topology of Fig. 2. Note that, with this connection, the three-phase machine becomes equivalent to a nonsymmetric two-phase machine (for example, the resistance of winding B is twice the resistance of winding A). The techniques developed in this paper can therefore be used for three-phase machines as well.

The objective of this paper is to explore issues in the design of a feedback controller for the concept shown in Fig. 1. The feasibility of utilizing relatively simple control laws is explored, including a standard proportional–integral control law (similar to the one used in [12]), an adaptive control law designed assuming a steady-state approximation of the system, and an adaptive control law based on the same assumption but adapting to uncertainties in the system as well. Experimental results show that several controllers can be successfully designed to regulate the voltage and frequency on the load while compensating for changes in speed and load.

II. Modeling and Parameter Estimation

For control purposes, it is useful to obtain a state-space model of the system. In [13], the following state-space model of a nonsymmetric two-phase induction machine was derived

$$\begin{pmatrix} L_A & & M_A & 0 \\ 0 & L_B & 0 & M_B \\ M_A & 0 & L_R & 0 \\ 0 & M_B & 0 & L_R \end{pmatrix} \frac{d}{dt} \begin{pmatrix} i_{SA} \\ i_{SB} \\ i_{RA} \\ i_{RB} \end{pmatrix} = \begin{pmatrix} v_{SA} - R_A i_{SA} \\ v_{SB} - R_B i_{SB} \\ -R_R i_{RA} - n_p\omega(L_R i_{RB} + M_B i_{SB}) \\ -R_R i_{RB} + n_p\omega(L_R i_{RA} + M_A i_{SA}) \end{pmatrix}. \quad (1)$$

Using a novel method based on a least squares algorithm, parameters were determined for the capacitor-start induction-run machine used in this paper and are given in Tables I and II.

Considering the operation with a resistive load R and a capacitor C connected in parallel with the generator, the system (1) can be expressed as

$$E\frac{d}{dt}(x) = Fx + Gu \quad (2)$$

where

$$E = \begin{pmatrix} L_A & 0 & M_A & 0 & 0 \\ 0 & L_B & 0 & M_B & 0 \\ M_A & 0 & L_R & 0 & 0 \\ 0 & M_B & 0 & L_R & 0 \\ 0 & 0 & 0 & 0 & C \end{pmatrix}, \quad x = \begin{pmatrix} i_{SA} \\ i_{SB} \\ i_{RA} \\ i_{RB} \\ v_{SB} \end{pmatrix}$$

$$F = \begin{pmatrix} -R_A & 0 & 0 & 0 & 0 \\ 0 & -R_B & 0 & 0 & 1 \\ 0 & -n_p\omega M_B & -R_R & -n_p\omega L_R & 0 \\ n_p\omega M_A & 0 & n_p\omega L_R & -R_R & 0 \\ 0 & 1 & 0 & 0 & -1/R_L \end{pmatrix}$$

$$G = \begin{pmatrix} 1 \\ 0 \\ 0 \\ 0 \\ 0 \end{pmatrix}, \quad u = v_{SA}. \quad (3)$$

In the Laplace domain, the vector transfer function $H(s)$ from $V_{SA}(s)$ to $X(s)$ is given by

$$H(s) = (Es - F)^{-1}G. \quad (4)$$

In particular, the scalar transfer function from $V_{SA}(s)$ to $I_{SA}(s)$ is

$$\frac{I_{SA}(s)}{V_{SA}(s)} = H_1(s) \quad (5)$$

where $H_1(s)$ is the first element of the vector $H(s)$. Similar relationships apply for the other elements of the state vector.

III. Determination of Operating Conditions

A. Viable Region Estimation

The next step of the study was to identify viable operating regions. A region is considered viable if more electrical power is produced than consumed. The size of the viable region is determined by several factors, including load, capacitance, and mechanical frequency. Once a viable region is identified, an operating point within the region may be selected. Operating points could be chosen to provide maximum power, to provide optimum efficiency, or to satisfy other design requirements.

The transfer function defined in (4) can be used to compute the power generated by the machine. Assuming that a sinusoidal voltage is applied to winding A

$$v_{SA}(t) = A\sin(\omega_e t). \quad (6)$$

TABLE I
PARAMETERS OBTAINED FROM AUXILIARY EXCITATION

R_A	L_A	R_R/L_R	M_A^2/L_R	M_AM_B/L_R
5.38 Ω	0.199 H	0.103 Ω/H	0.177 H	0.098 H

TABLE II
PARAMETERS OBTAINED FROM MAIN EXCITATION

R_B	L_B	R_R/L_R	M_B^2/L_R	M_AM_B/L
1.34 Ω	0.122 H	0.136 Ω/H	0.113 H	0.096 H

The steady-state current in winding A is given by

$$i_{SA} = A\,\mathrm{Re}\,[H_1(j\omega_e)]\sin(\omega_e t) + A\,\mathrm{Im}\,[H_1(j\omega_e)]\cos(\omega_e t). \tag{7}$$

Therefore, the active power absorbed by winding A is given by

$$P_A = \frac{A^2}{2}\mathrm{Re}\,[H_1(j\omega_e)]\,. \tag{8}$$

Similarly, the following power variables can be computed:

$$Q_A = \frac{-A^2}{2}\mathrm{Im}\,[H_1(j\omega_e)] \tag{9}$$

$$P_B = \frac{A^2}{2}\mathrm{Re}\,[H_2(j\omega_e)H_5(-j\omega_e)] \tag{10}$$

$$Q_B = \frac{-A^2}{2}\mathrm{Im}\,[H_2(j\omega_e)H_5(-j\omega_e)]\,. \tag{11}$$

The transfer functions involved are dependent on the electrical frequency, the mechanical frequency, the load resistance, and the capacitance. In order to restrict the design space, the electrical frequency was selected to be 60 Hz. This enables conventional consumer electronics to operate without the need for special power converters. The load resistance was chosen to be $R_L = 100\ \Omega$, which corresponds approximately to the nominal power level of the machine at 110 V_{rms} (note, however, that the voltage on the load was later reduced to 110 V_{pk} due to limitations of the test bed). A capacitance $C = 200\ \mu$F was selected based on an estimate of the reactive power requirements of the generating phase. These choices left the mechanical frequency ω as the only free parameter.

Values of P_A, Q_A, P_B, and Q_B (absorbed by the machine) were calculated for a range of ω, using the machine parameters from Tables I and II. The computation predicted a viable region just above the synchronous speed of the generator at 188.5 rad/s. The region was approximately 30 rad/s wide, and peak power was delivered at approximately 207 rad/s.

Experiments were then performed where phase A (auxiliary winding) of the induction generator was connected to the grid via a variac. The load was connected to phase B (main winding), and the voltage across the main winding was adjusted using the variac to 110 V_{pk}. The mechanical frequency of the machine was manually set using a laser tachometer, and the procedure was performed for ten speeds above the synchronous speed of the motor. At each point, the power consumption of the machine was measured using a Voltech PM1000 power analyzer.

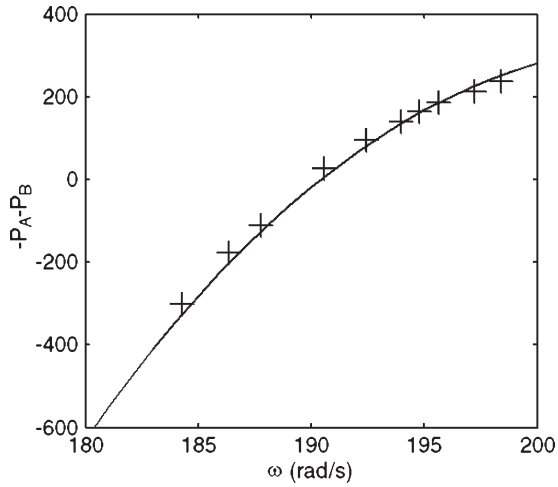

Fig. 3. Total power produced by the induction machine.

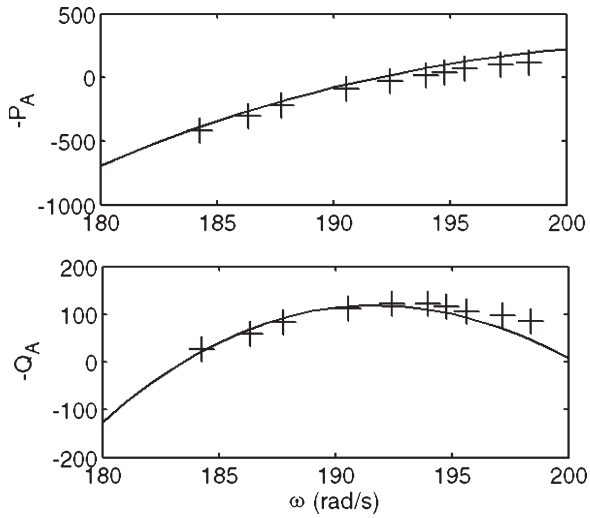

Fig. 4. Active and reactive powers produced by the auxiliary phase.

The experimental data are plotted along with the predicted values on Fig. 3. The total power generated by both phases of the machine, as computed by the formula, is shown as a solid curve. The region above 200 rad/s exceeded the ratings of the test bed and is not shown. The measured values are shown on Fig. 3 as + signs. The agreement between the computation and the data is very good.

The active and reactive powers absorbed by the excited phase (auxiliary winding) are shown in Fig. 4. It is important to note that the computation predicts that power can be either consumed or generated by the excited phase while the total power generated is positive.

B. Selection of Operation Point

Once the feasible region was identified, the next step was to choose an operating point within the region. As shown in Fig. 4, the point $P_A = 0$ appears within the range of viable speeds at approximately $\omega = 193.25$ rad/s. This setting was considered an attractive operating point because the excited phase did not consume or produce any real power and the amplifier used in the experiments was nonregenerative. In general, the

mechanical speed can be adjusted below this nominal operating point to draw additional power from the battery supplying the inverter or above it to generate more power and recharge the battery by using a bidirectional inverter in place of a power amplifier as used in the experiment.

IV. Control Development

In this section, methods are proposed to produce a controlled voltage across the generating phase of the machine. This problem presents several challenges. First, the system is highly resonant (computations show that it has a pair of poles near the $j\omega$-axis). Second, the transfer function of the system is highly dependent on the mechanical speed. Changes in this velocity can cause the system to depart significantly from original conditions. Finally, the model includes equations for the rotor currents, which cannot be measured in practice. Overall, the controller must function without the knowledge of these currents and with uncertainties in the machine parameters, speed, and load.

It was decided to explore the feasibility of relatively simple control laws that did not require a fifth-order observer for the system (3). Four controllers were considered: an open-loop controller, two adaptive controllers, and a PI controller. The first three controllers are designed to match the amplitude and phase of a reference signal. The ability to track both the amplitude and the phase is useful in order to synchronize the generator to the grid (synchronization would need to be manual for the open-loop controller). The PI controller is designed to only regulate the amplitude of the sinusoidal voltage (not the phase). This method is applicable to systems operating as stand-alone generators where phase is not a consideration.

The four methods are discussed in detail hereinafter, and all are based on the steady-state sinusoidal response of the system. The plant is thus represented by the frequency response $H_5(j\omega)$. The dynamics of the rotor are neglected, and the load and the speed are assumed constant. However, all closed-loop methods provide a certain degree of robustness to changes in these variables. In particular, one of the adaptive control laws estimates in real time the frequency response $H_5(j\omega)$.

A. Open-Loop Control

The system is assumed to be described by

$$y(t) = P(s)\left[u(t)\right] \tag{12}$$

where $y(t)$ is the plant output, $u(t)$ is the control input, and $P(s)[(\cdot)]$ denotes the time-domain output of the plant with transfer function $P(s)$. In this context, u is the voltage applied to the auxiliary phase (v_{SA}), and y is the voltage at the main phase (v_{SB}). The plant $P(s) = H_5(s)$ is assumed to be stable. The objective is for the plant output to track a sinusoidal reference signal

$$r(t) = r_c\cos(\omega_e t) + r_s\sin(\omega_e t) \tag{13}$$

where r_c, r_s are reference parameters determining the magnitude and phase of the reference signal and ω_e is the frequency of the reference signal. Specifically, $\sqrt{(r_s^2 + r_c^2)} = 110$ V, and $\omega_e = 2\pi 60$ (for 110 $V_{\rm pk}$ and 60 Hz).

The control signal is chosen to be

$$u(t) = u_c\cos(\omega_e t) + u_s\sin(\omega_e t) \tag{14}$$

where u_c, u_s are control parameters to be determined. For fixed control parameters, the steady-state output of the plant is

$$\begin{aligned} y_{ss} = {} & P_R\left(u_c\cos(\omega_e t) + u_s\sin(\omega_e t)\right) \\ & + P_I\left(-u_c\sin(\omega_e t) + u_s\cos(\omega_e t)\right) \end{aligned} \tag{15}$$

where P_R, P_I are the real and imaginary parts of the plant's frequency response evaluated at ω_e. It follows that $y_{ss}(t) = r(t)$ for all t if u_c, u_s are equal to the so-called nominal control parameters

$$\begin{pmatrix} u_c^* \\ u_s^* \end{pmatrix} = G^{*-1}\begin{pmatrix} r_c \\ r_s \end{pmatrix} \tag{16}$$

where G^* is given by

$$G^* = \begin{pmatrix} P_R & P_I \\ -P_I & P_R \end{pmatrix}. \tag{17}$$

In practice, (16) is implemented as

$$\begin{pmatrix} u_c \\ u_s \end{pmatrix} = G^{-1}\begin{pmatrix} r_c \\ r_s \end{pmatrix} \tag{18}$$

where G is an estimate of the matrix G^*. Estimates of P_R and P_I can be computed from the model (3) and (4) but depend on the speed and the load parameters.

Practically, this method consists simply in computing the gain and phase of the frequency response from v_{SA} to v_{SB} and adjusting the magnitude and phase of the voltage applied to the auxiliary winding so that the magnitude and phase of the voltage on the main winding take the desired value. No measurement of the voltage on the main winding is taken, so this purely open-loop method is highly vulnerable to errors in the plant model.

B. Adaptive Algorithm for Known Plant

A closed-loop adaptive algorithm is proposed to reduce the effect of uncertainties in the matrix G (including variations due to load and speed changes). The algorithm is the *inverse-G adaptive algorithm* of [14], which is a special case of the *filtered-X LMS algorithm* of signal processing. The method searches for control parameters that minimize the error between the reference signal and the plant output. For this purpose, it is convenient to define

$$r_v = \begin{pmatrix} r_c \\ r_s \end{pmatrix} \quad u_v = \begin{pmatrix} u_c \\ u_s \end{pmatrix} \quad w(t) = \begin{pmatrix} \cos(\omega_e t) \\ \sin(\omega_e t) \end{pmatrix} \tag{19}$$

so that, in steady state

$$r(t) = w^T(t)r_v \quad u(t) = w^T(t)u_v. \tag{20}$$

The adaptive algorithm for u_v is then defined as

$$\frac{d}{dt}\left(u_v(t)\right) = 2gG^{-1}w(t)\left(r(t) - y(t)\right) \tag{21}$$

where $g > 0$ is an arbitrary adaptation gain to be adjusted for optimal performance.

A motivation for (21) can be found using the theory of averaging. A simplified explanation follows. Approximating y by its steady-state value for fixed control parameters

$$r(t) - y(t) \simeq w^T(t)(r_v - G^* u_v). \tag{22}$$

Neglecting sinusoidal terms of frequency $2\omega_e$ (to be "averaged" by the differential equation for u_v), one has

$$2w(t)w^T(t) \simeq I \tag{23}$$

where I is the identity matrix. Therefore,

$$2w(t)\left(r(t) - y(t)\right) \simeq r_v - G^* u_v. \tag{24}$$

With these approximations,

$$\frac{d}{dt}\left(u_v(t)\right) = gG^{-1}G^*\left(u_v^* - u_v\right). \tag{25}$$

In ideal conditions ($G = G^*$),

$$\frac{d}{dt}\left(u_v(t)\right) = g\left(u_v^* - u_v\right) \tag{26}$$

so that the control vector converges to the nominal vector with the dynamics of two first-order systems with poles at $s = -g$.

An advantage of the algorithm is that convergence to the nominal vector still occurs if $G \neq G^*$, as long as stability is preserved. In general, the stability of the system is determined by the roots of

$$\det(sI - gG^{-1}G^*) = 0 \tag{27}$$

which remain in the open left-half plane if G is sufficiently close to G^*. In other words, the method assumes a known plant (i.e., known matrix G) but tolerates uncertainties in G (as opposed to the open-loop method that does not).

In summary, the algorithm is defined by (19)–(21). The matrix G is obtained from the model (3) and (4) and the estimated parameters (as well as a nominal value of the speed). The free parameter g can be adjusted to place the poles of the approximate system at $s = -g$.

C. Adaptive Algorithm With Plant Adaptation

The second adaptive algorithm is designed to identify the plant parameters, rather than to be robust to uncertainties in their estimates. It is a simplified form of the algorithm of [15], which is a periodic disturbance rejection algorithm. Simplification occurs because the reference parameters r_c, r_s are known, as opposed to the disturbance rejection case. The algorithm is obtained by defining a vector of plant parameter estimates x, whose nominal value is

$$x^* = \begin{pmatrix} P_R \\ P_I \end{pmatrix}. \tag{28}$$

The control law is defined from the parameter estimates as if they were the nominal parameters, i.e.,

$$u_v = G^{-1} r_v \tag{29}$$

with

$$G = \begin{pmatrix} x_1 & x_2 \\ -x_2 & x_1 \end{pmatrix}. \tag{30}$$

Then, (24) can be rewritten as

$$2w(t)\left(r(t) - y(t)\right) \simeq r_v - Wx^* \tag{31}$$

where

$$W = \begin{pmatrix} u_c & u_s \\ -u_s & u_c \end{pmatrix} = \frac{1}{x_1^2 + x_2^2}\begin{pmatrix} x_1 r_c - x_2 r_s & x_1 r_s + x_2 r_c \\ x_1 r_s + x_2 r_c & -x_1 r_c + x_2 r_s \end{pmatrix}. \tag{32}$$

Next, define the error signal

$$e_a = Wx - r_v + 2w(t)\left(r(t) - y(t)\right). \tag{33}$$

Within approximations made earlier, the error signal is equal to

$$e_a = W(x - x^*) \tag{34}$$

so that the error vector e_a is related linearly to the parameter error, and standard gradient or least squares algorithms can be used for parameter estimation [16]. For example, a gradient algorithm is given by

$$\frac{d}{dt}(x) = -gW^T e_a \tag{35}$$

where $g > 0$ is an adaptation gain to be selected arbitrarily. The algorithm is nonlinear because W is a function of x. However, it is guaranteed to be stable because

$$\begin{aligned} \frac{d}{dt}\|x - x^*\|^2 &= -2g(x - x^*)^T W^T e_a \\ &= -2g\left(W(x - x^*)^T W(x - x^*)\right) \\ &= -2g\left\|W(x - x^*)\right\|^2 \leq 0. \end{aligned} \tag{36}$$

Furthermore, the parameter error and the tracking error converge to zero if W is nonsingular, which requires that r_c or $r_s \neq 0$. There is a potential problem in the computation of u if $x_1^2 + x_2^2 = 0$, but it can be avoided by replacing the computation of u_v by

$$u_v = \frac{1}{\max\left(\varepsilon, x_1^2 + x_2^2\right)}\begin{pmatrix} x_1 r_c - x_2 r_s \\ x_1 r_s + x_2 r_c \end{pmatrix} \tag{37}$$

where ε is a small positive number such that $\varepsilon < x_1^{*2} + x_2^{*2}$.

Unfortunately, this method does not give a simple way to relate the parameter g to the poles of the system, so the parameter must be tuned experimentally.

TABLE III
NAMEPLATE DATA OF PRIME MOVER

Power	Speed	Phases	Hz	Voltage
1/2 HP	3450 rpm	3	60 Hz	208-230 V

D. PI Control

The previous three controllers tracked the magnitude and phase of a reference sinusoid. A different controller design can be obtained when the phase is unimportant. A straightforward approach is to calculate the difference between the measured amplitude and the reference amplitude and to apply the error to a PI controller.

The concept assumes that a measurement of the amplitude of the generated voltage is available. A typical way to estimate the amplitude of a generated voltage is envelope detection. This method introduces a delay and a nonlinearity in the system. Madawala *et al.* [12] use an rms detector without providing any detail of the algorithm. Here, we propose a simple and effective method that exploits the fact that the voltage on the main winding is produced by the excitation voltage, whose frequency and phase are known exactly.

An estimate of the generated voltage is defined as

$$\hat{y}(t) = y_c \cos(\omega_e t) + y_s \sin(\omega_e t) \tag{38}$$

where the values of y_c and y_s are updated with

$$\frac{d}{dt}(y_c) = g\left(y(t) - \hat{y}(t)\right)\cos(\omega_e t) \tag{39}$$

$$\frac{d}{dt}(y_s) = g\left(y(t) - \hat{y}(t)\right)\sin(\omega_e t) \tag{40}$$

and $g > 0$ is an adjustable gain (the gains g of this paper are all adjustable gains that have similar purposes but can take different values). The algorithm can be analyzed as the algorithm of Section IV-B, and its averaged approximation is composed of two first-order systems with poles at $s = -g$. The estimate of the amplitude is simply $Y = \sqrt{(y_c^2 + y_s^2)}$.

Even with a good amplitude detector, the design of a PI control law is not obvious because there is not a linear time-invariant system description relating the *amplitude* of the input sinusoid to the *amplitude* of the output. Thus, the gains of the PI controller were tuned experimentally.

V. EXPERIMENTAL RESULTS

A. Experimental Setup

An experimental test bed was assembled to test the control methods described in Section IV. The test bed consisted of a two-pole induction motor connected to a four-pole generator via a spider coupling. Both machines were manufactured by the Worldwide Electric Corporation. The prime mover had the nameplate data given in Table III.

The three-phase voltage required by the prime mover was provided by a GE 300 Mini adjustable frequency drive. The 300 Mini is a V/f drive, and therefore, the speed of the motor was not regulated under varying torque. Fig. 5 shows the speed response due to a 110 $V_{\rm pk}$ step in the generated voltage. The measurements were obtained using a Compact Instruments laser tachometer. The data were filtered using a six-pole Butterworth low-pass filter with a 40-Hz cutoff frequency. The variation of speed of the prime mover shown in Fig. 5 was not considered in the control development and represents an uncertainty to which the algorithms should be proved to be robust.

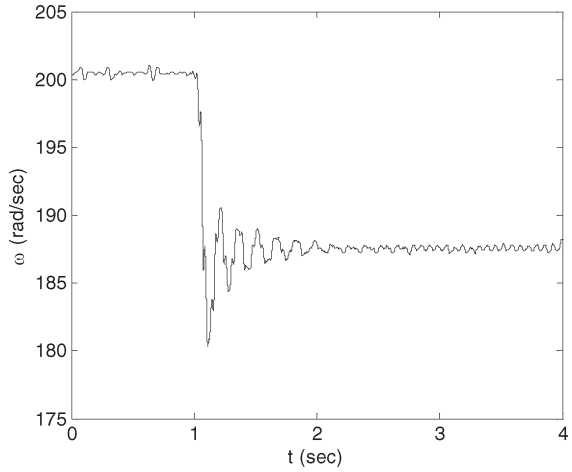

Fig. 5. Speed response to a step change in electrical load.

TABLE IV
NAMEPLATE DATA OF GENERATOR

Power	Speed	Phases	Hz	Voltage
1/3 HP	1725 rpm	1	60 Hz	115/230 V

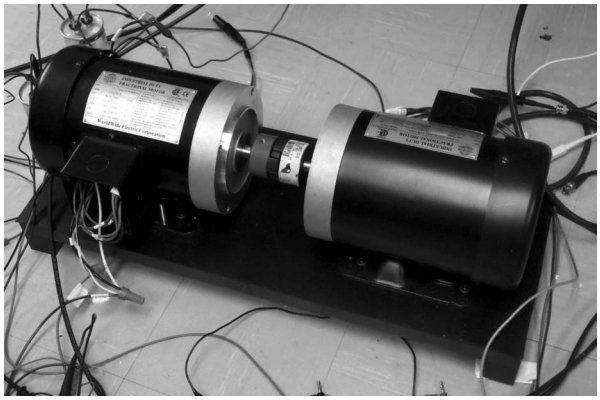

Fig. 6. Experimental setup. (Left) Generator is mechanically coupled to the (right) drive.

The generator under test was a split-phase motor with the nameplate data given in Table IV. The start capacitor was removed in order to provide access to the auxiliary phase of the machine. Both machines were fastened to a heavy metal plate for stability. The setup is shown in Fig. 6.

The excitation signal was generated using the digital-to-analog converter of a dSPACE DS1104 controller board and passed to a power amplifier. The generated voltage was measured using an analog-to-digital converter on the DS1104. The reference was set to $r_c = 110$ and $r_s = 0$. Recall that the desired 110 $V_{\rm rms}$ voltage was scaled back to 110 $V_{\rm pk}$ due to limitations of the power amplifier used in the experiment.

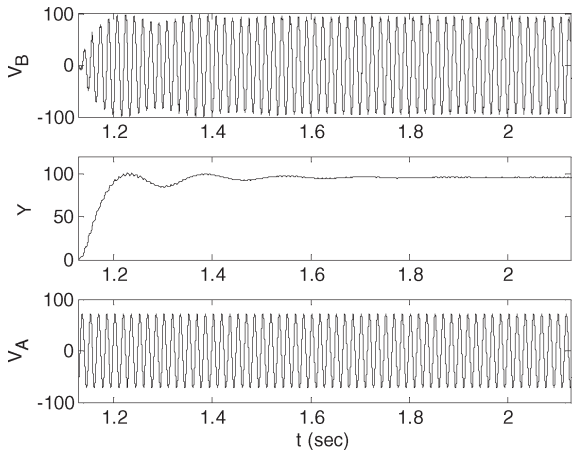

Fig. 7. Response with open-loop control.

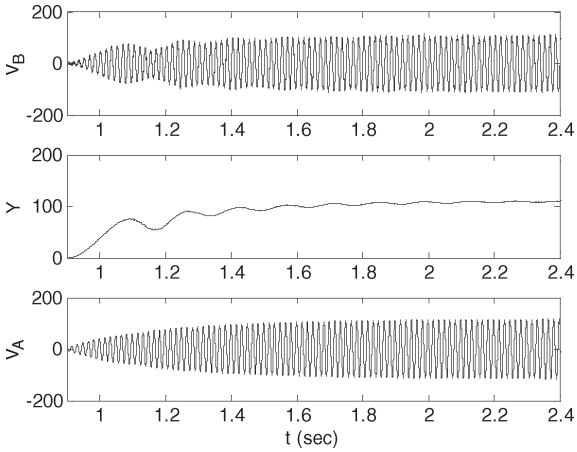

Fig. 8. Response of the adaptive algorithm for known plant to a step change in voltage.

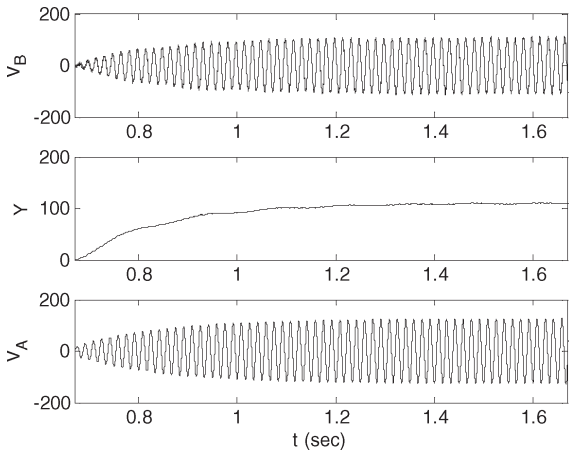

Fig. 9. Response of the adaptive algorithm for known plant to a step change in voltage at a slower speed. Transients introduced by the drive are reduced.

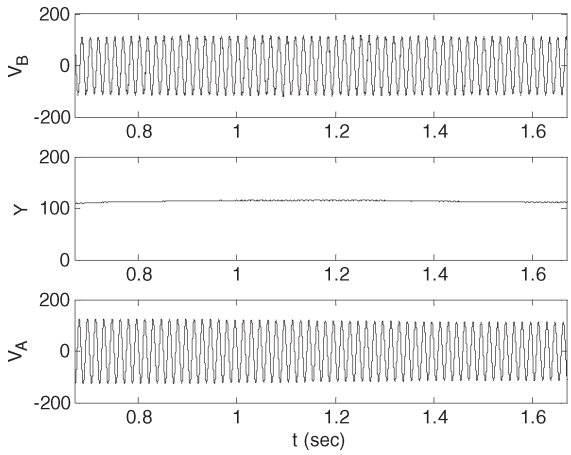

Fig. 10. Response of the adaptive algorithm for known plant to a disturbance in rotor velocity.

B. Open-Loop Control

The open-loop control method was implemented first. The results of the experiment are shown in Fig. 7. An estimate of the amplitude of the generated voltage, Y, is included in the plot. The estimate was calculated using (39) and (40) but was not used in the control law. Note that the model predicts an overdamped behavior in this operating condition, but the system exhibits slightly underdamped responses. This behavior is due to oscillations in the speed of the generator–motor system shown in Fig. 5.

C. Adaptive Algorithm for Known Plant

Next, the adaptive method for the known plant was coded in C and loaded on the dSPACE system. The adaptation gain was set to $g = 3$. The results are shown in Fig. 8. The experiment was repeated at a slower speed to obtain the response shown in Fig. 9. The response at lower speed is less oscillatory. Larger gains were found to improve the transient response of the generator but introduce steady-state oscillations to the output.

It is also informative to examine the response of the algorithm to variations in the plant parameters. The generator was started and allowed to reach steady state at a speed of 1800 r/min. The mechanical frequency was increased to 2160 r/min, and the system was allowed to return to the steady state. The resulting transients are shown in Fig. 10 and were found to be small. The maximum voltage deviation is 5%.

D. Adaptive Algorithm With Plant Adaptation

The third experiment implemented on the system was the adaptive algorithm for an unknown plant. The adaptation gain was set to $g = 0.0001$. The initial values of the parameters x_1 and x_2 were estimated using the real and imaginary parts of the frequency response. The response of the controller to a step reference is shown in Fig. 11. The peak voltage is approximately 148 V and is too high.

The adaptive action of this method is apparent in Fig. 12. The estimates of the plant transfer function converge to $x_1 = -0.54$ and $x_2 = -0.77$. A larger adaptive gain causes these estimates to converge quicker but introduces more overshoot to the system.

The experiments were repeated at a slower speed to reduce drive dynamics. The step response of the controller is shown in Fig. 13. The overshoot is reduced to approximately 5%.

The controller's response to a step change in plant parameters was also tested by increasing the speed of the generator from 30 to 36 Hz. The results are shown in Fig. 14.

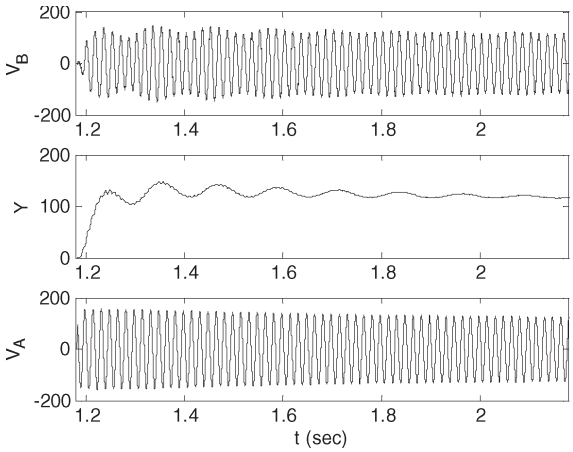

Fig. 11. Response of the adaptive algorithm with plant adaptation to a step change in voltage.

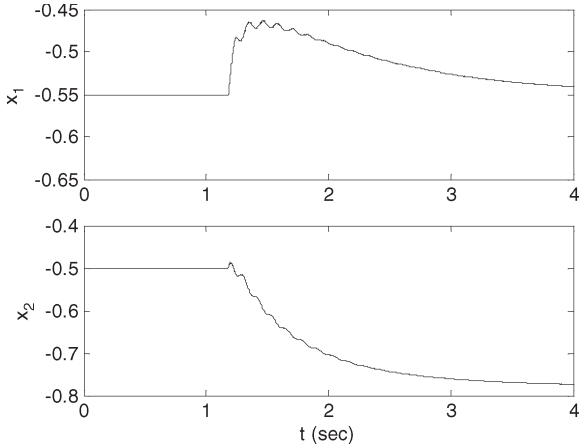

Fig. 12. Parameter adaptation due to a step change in voltage.

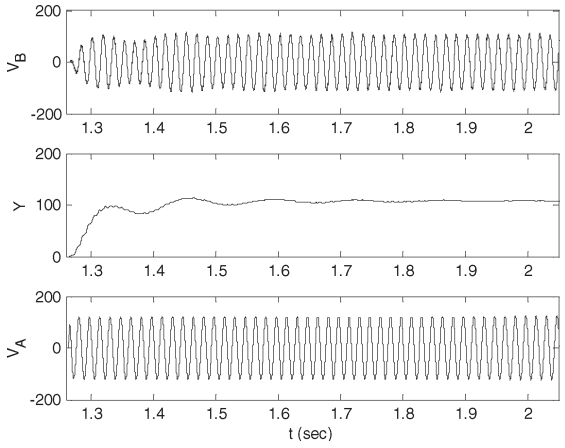

Fig. 13. Response of the adaptive algorithm with plant adaptation to a step voltage at slower speed. Transients introduced by the drive are reduced.

E. PI Control

The PI control method was implemented in a similar fashion. The gain used in the amplitude estimator was chosen to be $g = 150$. The feedback gains were selected to be $k_P = 0.5$ and $k_I = 6.5$. The results of the experiment are shown in Fig. 15. Large gains were found to cause steady-state oscillations in the output voltage. Once again, the experiment was repeated at a slower speed. The results of the slower experiment are shown in Fig. 16. As in previous experiments, a slower speed reduces the oscillations.

The response of the PI controller to a change in the plant parameters was also investigated. Fig. 17 shows the response of the system to a 20% increase in speed at $t = 1.5$ s. Since the action of the controller is faster than the acceleration of the prime mover, there is no significant change in the generated voltage.

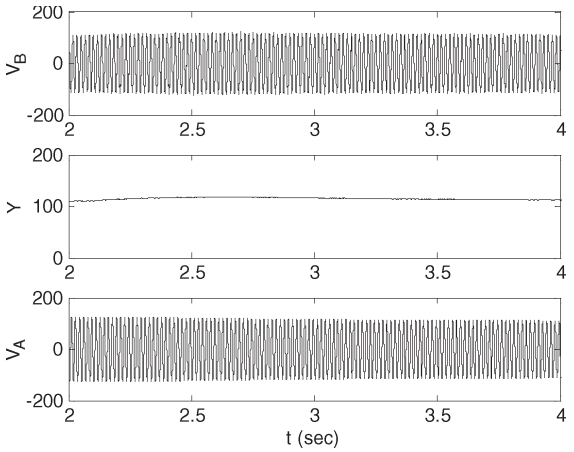

Fig. 14. Response of the adaptive algorithm with plant adaptation to a disturbance in speed.

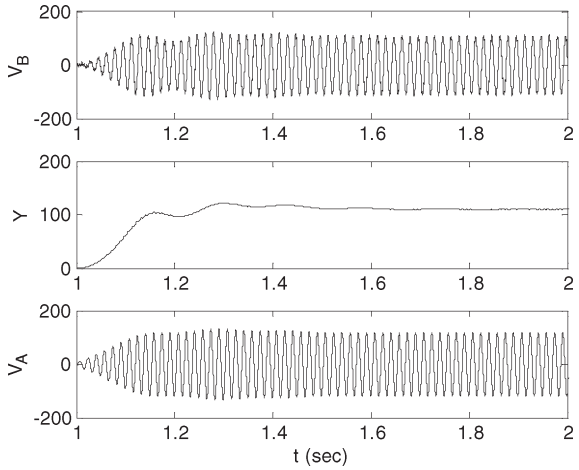

Fig. 15. Response of the PI controller to a step change in voltage.

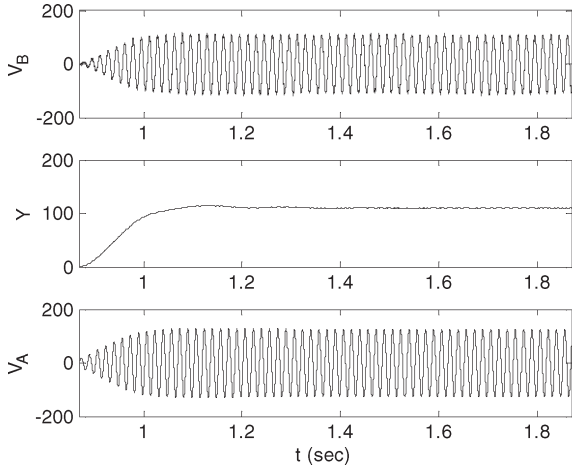

Fig. 16. Response of the PI controller to a step change in voltage at slower speed.

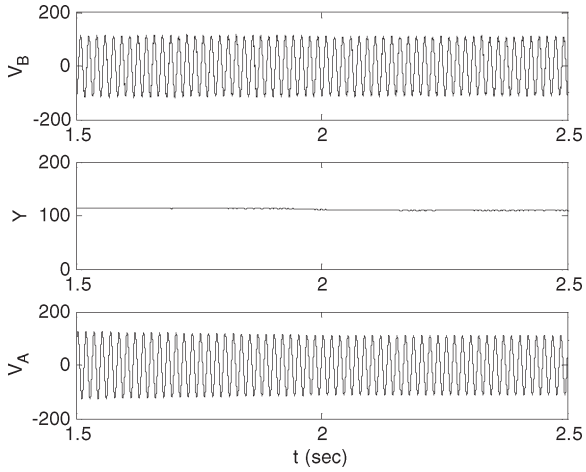

Fig. 17. Response of the PI controller to a disturbance in rotor velocity.

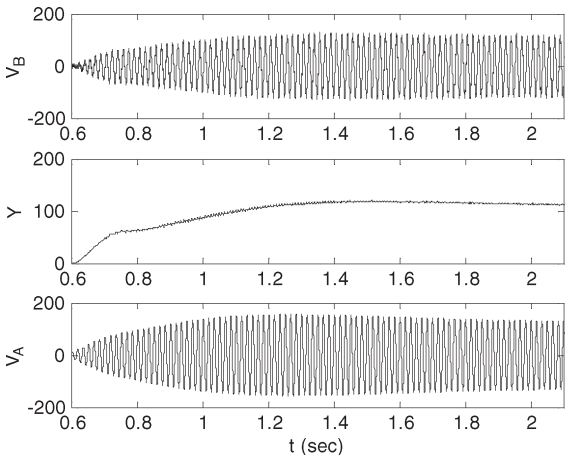

Fig. 18. Response of the PI controller to a step change in voltage with an inductive load.

A final experiment was performed to examine the behavior of the generator under different loading conditions. The 100-Ω load resistor was replaced with a universal motor, which also requires reactive power. Fig. 18 shows the response of the system initialized from zero. The response with this load is improved because the load increases gradually, eliminating some of the overshoot. The same gains were used for each of these experiments.

VI. Conclusion

This paper has examined the problem of producing a controlled voltage from a squirrel-cage induction machine using the inverter-assisted topology. The state-space model of a nonsymmetric two-phase machine was presented, including an RC load connected across the main winding. Identified parameters were used to estimate viable operating regions, and it was concluded that power could be produced in a limited region above the synchronous speed of the motor. Power was produced by both phases of the machine in most of the operating region but was absorbed by the auxiliary winding in the low end of the speed range. The point with zero auxiliary power was arbitrarily chosen as the operating point for the experiments, considering experimental constraints.

Four control methods were investigated. The open-loop control method exhibited oscillations and could not track a reference voltage. The three closed-loop algorithms were able to track a specified reference and were robust to 20% increases in speed. However, overshoot and oscillations were observed in some cases and were found to be reduced at lower speed. In situations where phase is not a consideration, the PI control method was found preferable. It responded faster than either adaptive methods.

In all cases, the variation of the speed of the prime mover was a limiting factor of the transient performance. The induction motor and V/f drive used as a prime mover in the experiments provided no speed tracking and little damping. Improvements could be obtained by regulating the speed or perhaps simply by increasing the inertia of the system. Further research could also focus on methods to improve the transient response of the motor–generator set by using a model of the prime mover in the control law and a speed measurement. However, such methods would be significantly more complicated than the algorithms presented in this paper.

References

[1] D. W. Novotny, D. J. Gritter, and G. H. Studman, "Self-excitation in inverter driven induction machines," *IEEE Trans. Power App. Syst.*, vol. 96, no. 4, pp. 1117–1125, Jul. 1977.

[2] S. S. Murthy, "A novel self-induced self-regulated single phase induction generator. I. Basic system and theory," *IEEE Trans. Energy Convers.*, vol. 8, no. 3, pp. 377–382, Sep. 1993.

[3] S. S. Murthy, H. C. Rai, and A. K. Tandon, "A novel self-excited self-regulated single phase induction generator. II. Experimental investigation," *IEEE Trans. Energy Convers.*, vol. 8, no. 3, pp. 383–388, Sep. 1993.

[4] M. Bodson and O. Kiselychnyk, "Analysis of triggered self-excitation in induction generators and experimental validation," *IEEE Trans. Energy Convers.*, vol. 27, no. 2, pp. 238–249, Jun. 2012.

[5] O. Ojo, "The transient and qualitative performance of a self-excited, single-phase induction generator," *IEEE Trans. Energy Convers.*, vol. 110, no. 3, pp. 493–501, Sep. 1995.

[6] O. Ojo and B. Gonoh, "A controlled stand-alone single-phase induction generator," in *Proc. Power Electron., Drives Energy Syst. Ind. Growth*, 1996, vol. 2, pp. 694–699.

[7] O. Ojo, "Performance of self-excited single-phase induction generators with shunt, short-shunt and long-shunt excitation connections," *IEEE Trans. Energy Convers.*, vol. 11, no. 3, pp. 477–482, Sep. 1996.

[8] O. Ojo, O. Omozusi, and A. A. Jimoh, "Performance of an autonomous single-phase induction generator with a bidirectional PWM inverter-battery system in the auxiliary winding," in *Proc. IEEE Int. Symp. Ind. Electron.*, 1998, vol. 1, pp. 306–311.

[9] O. Ojo, O. Omozusi, A. Ginart, and B. Gonoh, "The operation of a stand-alone single-phase induction generator using a single-phase, pulse-width modulated inverter with a battery supply," *IEEE Trans. Energy Convers.*, vol. 14, no. 3, pp. 526–531, Sep. 1999.

[10] O. Ojo, "The operation of an inverter-assisted single-phase induction generator," *IEEE Trans. Ind. Electron.*, vol. 47, no. 3, pp. 632–640, Jun. 2000.

[11] O. Ojo, O. Omozusi, M. Omoigui, and A. A. Jimoh, "Parameter estimation of single-phase induction machines," in *Conf. Rec. IEEE IAS Annu. Meeting*, 2001, pp. 2280–2287.

[12] U. K. Madawala, T. Geyer, J. B. Bradshaw, and D. M. Vilathgamuwa, "Modeling and analysis of a novel variable-speed cage induction generator," *IEEE Trans. Ind. Electron.*, vol. 59, no. 2, pp. 1020–1028, Feb. 2012.

[13] M. Myers, M. Bodson, and F. Khan, "Determination of the parameters of non-symmetric induction machines," in *Proc. Appl. Power Electron. Conf.*, Forth-Worth, TX, 2011, pp. 1028–1033.

[14] B. Wu and M. Bodson, "Multi-channel active noise control for periodic sources—Indirect approach," *Automatica*, vol. 40, no. 2, pp. 203–212, Feb. 2004.

[15] S. Pigg and M. Bodson, "Adaptive algorithms for the rejection of sinusoidal disturbances acting on unknown plants," *IEEE Trans. Control Syst. Technol.*, vol. 18, no. 4, pp. 822–836, Jul. 2010.

[16] S. Sastry and M. Bodson, *Adaptive Control: Stability, Convergence, and Robustness*. Englewood Cliffs, NJ: Prentice-Hall, 1989.

Max Myers received the B.S. degree in engineering from Harvey Mudd College, Claremont, CA, in 2009.

He specializes in the control of electronic drives and electrical machines. Since 2010, he has been a Power Electronics Engineer with Boulder Wind Power, Boulder, CO. He is primarily responsible for power converter simulation and embedded software design at Boulder Wind Power.

Marc Bodson received the degree of Ingénieur Civil Mécanicien et Electricien from the Université Libre de Bruxelles, Brussels, Belgium, in 1980, the M.S. degrees in electrical engineering and computer science and aeronautics and astronautics from the Massachusetts Institute of Technology, Cambridge, in 1982, the Ph.D. degree in electrical engineering and computer science from the University of California, Berkeley, in 1986.

He is currently a Professor of Electrical and Computer Engineering with the University of Utah, Salt Lake City. He was the Chair of the Department of Electrical and Computer Engineering between July 2003 and October 2009.

Prof. Bodson was the Editor-in-Chief of the IEEE TRANSACTIONS ON CONTROL SYSTEMS TECHNOLOGY between January 2000 and December 2003.

Faisal Khan received the B.Sc. degree in electrical engineering from Bangladesh University of Engineering and Technology, Dhaka, Bangladesh, in 1999, the M.S. degree in electrical engineering from Arizona State University, Phoenix, in 2003, and the Ph.D. degree in electrical engineering from the University of Tennessee, Knoxville, in 2007.

From 2007 to 2009, he was with the Electric Power Research Institute as a Senior Power Electronics Engineer. Since 2009, he has been with the Department of Electrical and Computer Engineering, University of Utah, Salt Lake City, as an Assistant Professor. His major area of interest is high-power capacitor-clamped converters. However, since his appointment at the university, he has extended his research into the field of power converter reliability prediction and cell level power converter design for photovoltaics, particularly multijunction solar cells. In addition, he is also involved with renewable energy research, including wind energy harvesting using split-phase induction generators and grid-tied energy storage.

Dr. Khan is a member of the IEEE Power Electronics Society, IEEE Industry Applications Society (IAS), and IEEE Industrial Electronics Society. He was the recipient of the 2007 IEEE IAS First Prize Paper Award for his contribution to high-power modular multilevel dc–dc converters. He is the Award Chair of IEEE Energy Conversion Congress and Exposition 2012 and the General Chair of IEEE Control and Modeling for Power Electronics 2013 in Salt Lake City.